# Modeling the Location and Shape of the Magnetopause Using Machine Learning Methods

M. Aghabozorgi Nafchi, F. Němec, G. Pi, Z. Němeček, J. Šafránková, K. Grygorov
Charles University, Faculty of Mathematics and Physics, Prague, Czech Republic.

J. Šimůnek
Institute of Atmospheric Physics of the Czech Academy of Sciences, Prague, Czech Republic.

**Abstract.** Empirical models for predicting the location of the magnetopause currently in use typically rely on the identification of individual magnetopause crossings, and their fitting by a predefined magnetopause shape. Although the assumed analytical shape formula may be rather complicated and general, it represents a principal apriori limitation of the model. We remove this limitation by applying an approach based on an artificial neural network. A large data set of about 15,000 subsolar magnetopause crossings is used for the training, resulting in a direct data-driven model predicting the magnetopause radial distance as a function of relevant solar wind parameters without any additional assumptions. The model performance is evaluated using the testing data set of magnetopause crossings and by a comparison with a former widely used empirical model.

## Introduction

Magnetopause is a dynamic boundary that separates the Earth's magnetic field from the shocked solar wind, protecting the Earth from this continuous stream of charged particles. The shape and location of the magnetopause are strongly influenced both by upstream solar wind and internal conditions within the magnetosphere [*Němeček et al.*, 2020]. Accompanied by the first observations of the magnetopause location [*Cahill and Amazeen*, 1963] using the three-component magnetometer carried by the Explorer 12 spacecraft, the magnetohydrodynamic (MHD) approach established a basic understanding of the interaction of the Earth's magnetic field with the solar wind [*Spreiter et al.*, 1966]. An empirical magnetopause model based on the identified crossings was offered by *Fairfield* [1971]. Since then, an increasing number of identified magnetopause crossings and continuous monitoring of the corresponding solar wind parameters gradually helped to constructed more advanced magnetopause models.

The main parameter affecting the position of the magnetopause is upstream dynamic pressure [*Formisano et al.*, 1979; *Petrinec and Russell*, 1996; *Lu et al.*, 2011; *Boardsen et al.*, 2000]. Interplanatary Magnetic Field (IMF) $B_z$ component is believed to be the second most influential factor determining magnetopause position which is discussed by *Sibeck et al.* [1991]. However, the large data set of magnetopause crossings obtained by the Interball spacecraft has revealed apparently no dependence of the subsolar magnetopause to the IMF $B_z$ [*Verigin et al.*, 2009]. Some recent studies suggest that it may be the IMF magnitude actually playing the role [*Li et al.*, 2023].

In addition to the IMF $B_z$ and IMF strength, the IMF cone angle appears to be another factor affecting the magnetopause location [*Dušík et al.*, 2010]. According to *Case and Wild* [2013], the IMF clock angle has no influence on the magnetopause location. However, the statistical analysis by *Nguyen et al.* [2021a] and *Nguyen et al.* [2021b] demonstrates the effect of IMF $B_y$ component in the flaring area. MHD simulations further indicate that magnetopause cross-section is extended along (or opposite) to the IMF direction and as compared to the direction perpendicular to the IMF [*Lu et al.*, 2013; *Liu et al.*, 2015]. Despite large experimental uncertainties, this seems to be confirmed by analyses of large magnetopause crossing data sets [*Lavraud et al.*, 2013; *Aghabozorgi et al.*, 2023].

A significant effort, both theoritical and experimental, as been made to explore the shape of the magnetopause in response to the dipole tilt angle [*Boardsen et al.*, 2000; *Tsyganenko*, 1998; *Eastman et al.*, 2000]. The significance of dipole tilt angle at higher latitudes was convinceingly demonstrated by *Šafránková et al.* [2005]. More sophisticated mathematical form describing the three-dimentional mag-

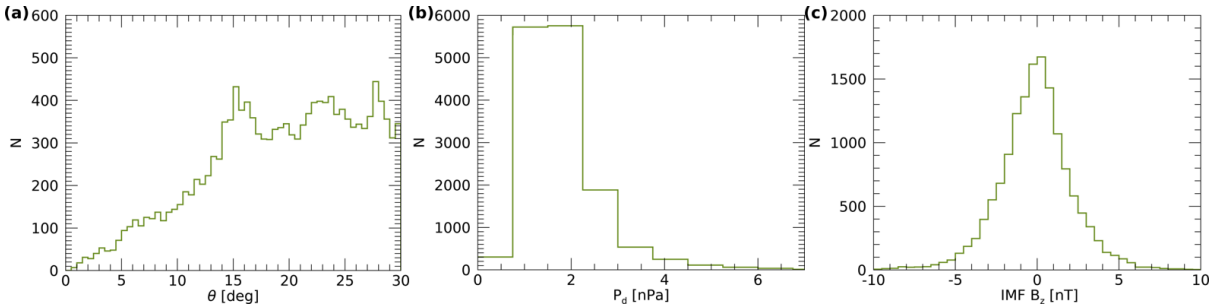


**Figure 1.** Histograms of parameters corresponding to the analyzed magnetopause crossings. (a) The angle $\theta$ between the crossing positional vector and the the direction toward the impinging solar wind. (b) Solar wind dynamic pressure. (c) IMF $B_z$.

netopause shape was eventually developed by *Lin et al.* [2010]. *Li et al.* [2023] designed an interpretable machine learning procedure determining the effects of interplanetary parameters on the magnetopause location.

In this study, we use a database of about 15,000 low-latitude dayside magnetopause crossings in the subsolar region to demonstrate the feasibility of the Neural Network (NN) modeling of the magnetopause location. Three model parameters are used: solar wind dynamic pressure ($p_d$), IMF $B_z$, and the angle between the magnetopause crossing positional vector and the the direction toward the impinging solar wind, assuming thus the cylindrical symmetry. The NN output, i.e., directly the model magnetopause crossing radial distance, is compared with the *Shue et al.* [1998] model, which uses the same parameterization. The used data set is described in the data section. The approach employed for data processing and the results obtained are presented and discussed in the results and discussion sections, respectively. Finally, the conclusion section provides the overview of main results.

## Data Set

Our full database comprises 49,638 magnetopause crossings identified in the THEMIS A–E, Geotail, Magion 4, and Interball satellites obtained between 1995 and 2020. An automated routine of finding simultaneous changes of magnetic field and plasma parameters [*Němeček et al.*, 2016] is used for identification of the magnetopause crossings in the THEMIS data. The identified crossings were carefully examined visually to remove false positives. The magnetopause crossings in the data measured by other spacecraft were analyzed manually [*Šafránková et al.*, 2002].

However, due to the limited apogee distance of the THEMIS spacecraft and the related insufficient sampling of large distances and possible sampling bias, only subsolar magnetopause crossings are used in the present study. These are selected based on the condition $\theta < 30^\circ$, with $\theta$ being the angle between the positional vector of a given crossing and the direction toward the impinging solar wind. This leaves us with as many as 14,781 magnetopause crossings. To each of the crossings, the corresponding solar wind parameters are attributed based on the Wind spacecraft measurements and a two-step propagation method by *Šafránková et al.* [2002]. As this is only an initial study of the possible usage of the NN modeling approach, we assume a simple magnetopause distance parameterization by $p_d$, $B_z$, and $\theta$, i.e., the same as in a widely used *Shue et al.* [1998] empirical model. The distribution of these three parameters for the analyzed magnetopause crossings is shown in Figure 1, representing the number of crossings at individual parameter intervals. It can be seen that, due to geometrical reasons, most magnetopause crossings are obtained at larger $\theta$ values. The distribution of $p_d$ has a rather long tail, extending to dynamic pressures as high as 7 nPa. On the other hand, the distribution of IMF $B_z$ is quite symmetric and roughly Gaussian-like.

## Neural Network Model

Artificial neural networks (ANNs) are intricate systems comprised of basic processing units referred to as "neurons." These neurons perform computations on their respective localized data while simultaneously communicate with other interconnected elements. While ANNs drew their initial inspiration from the structural attributes of the human brain, the design and configuration of processing elements and network architectures have significantly departed from their biological origins.

Although a diverse array of network types and structures has emerged within the realm of ANNs [*McCulloch and Pitts*, 1943], the fundamental principles remain remarkably akin. Each neuron within the network possesses the capability to accept input signals, carry out processing tasks on them, and subsequently transmit an output signal. Every neuron establishes connections, minimally with one other neuron, and each of these connections is assessed using a real number referred to as the weight coefficient. This weight coefficient quantifies the significance or importance of the specific connection within the neural network [*Svozil et al.*, 1997]. The primary strength of neural networks lies in their ability to utilize latent, previously unknown information contained within data, even though they cannot extract this information directly. This process of uncovering this hidden knowledge is referred to as neural network training. In mathematical terms, learning involves the adjustment of weight coefficients to satisfy specific conditions. There are two principal types of training processes: supervised and unsupervised training. In supervised training, as seen in the case of multi-layer feed-forward (MLF) neural networks, the network possesses knowledge of the desired output. Consequently, the adaptation of weight coefficients aims to minimize the disparity between the calculated and desired outputs. Unsupervised training, on the other hand, focuses on a different approach. Unsupervised training operates on the premise that the desired output is unknown. Instead, the system is presented with a collection of data instances (patterns) and is allowed to autonomously converge to a stable state through a series of iterations [*Kohonen*, 1989].

MLF neural networks are the most popular neural networks which are trained with a back-propagation learning algorithm. A MLF neural network consists of input, hidden, and output layers. Each neuron in a particular hidden layer is connected with all neurons in the next layer. The connection between each two neurons is characterized by the weight coefficient, reflecting the degree of importance of the given connection. For training and prediction of the MLF neural network, training and test sets are needed. The training mode begins with arbitrary (random) values of the weights and proceeds iteratively. During each iteration, the network adjusts the weights in order to reduce the error. As the iterative process of incremental adjustment continues, the weights gradually converge to the locally optimal set of values. In our study, the IDLmlFeedForwardNeuralNetwork built-in function in IDL software is used with three input layer, 2 hidden layers of 30 and 15 neurons, respectively, and one output. Our data set of subsolar magnetopause crossings is diveded into traning and testing subsets (80% and 20% of data points, respectively). The three inputs are same parameters as in the *Shue et al.* [1998] model. The used activation function is IDLmlafArcTan and the used optimizer is IDLmloptAdam with a learning rate of 0.0002. The neural networks is trained using 10,000 iterations, and it effectively converges well before that.

## Results

Green dots in Figure 2 represent the projections of the magnetopause crossings to the $\rho - x$ plane, where $x$ is the axis pointing toward the direction of the impinging solar wind and $\rho = \sqrt{y^2 + z^2}$. The blue curve corresponds to the NN-predicted magnetopause location for selected values of the controlling parameters, approximately corresponding to the median values over the data set ($p_d = 1.63$ nPa, IMF $B_z = 0$). The red dash-dotted curve corresponds to the NN model extrapolation to the $\theta$ values beyond the training data set. We note the small jump roughly in the middle of the blue curve. It is likely an artifact of the neural network configuration, but we do not have any clear explanation for it at the moment.

Figure 3a represents a direct one-to-one comparison between the magnetopause distances predicted

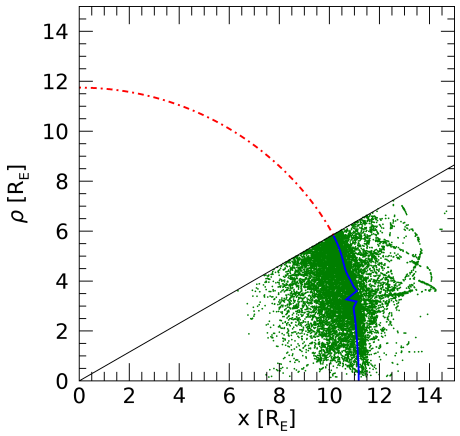


**Figure 2.** Schematic view of the model performance in terms of the magnetopause shape. The green dots correspond to the projections of the observed magnetopause crossings to $\rho - x$ plane. The blue curve corresponds to the model magnetopause distance obtained for the median value of the dynamic pressure and IMF $B_z = 0$. The red curve shows the model extrapolation beyond the $\theta$ angles in the training data set.

by the NN model and the observed magnetopause distances. Each green point represents a single magnetopause crossing, the solid blue line depicts an exact 1:1 dependence. Despite the substantial scatter indicating a non-perfect model performance, the model and observed distances have correlation of about 0.76, corresponding to reasonably good agreement. Nevertheless, it can be seen that the model tends to overpredict the radial distances for the near magnetopause crossings ($r_{obs} \lesssim 10.5\ R_E$), while it tends to underpredict the radial distances for the far magnetopause crossings ($r_{obs} \gtrsim 12\ R_E$). In other words, although the model general trend is quite correct, it is not as steep as it perhaps should be given the individual data points. However, for the distances more than $12 R_E$, majority of the crossings are located below the blue line. Figure 3b shows the histogram of differences between the observed and model magnetopause radial distances by the black line. For comparison, the red line shows the histogram of differences between the observed and model magnetopause radial distances obtained by the *Shue et al.* [1998] empirical magnetopause model evaluated using the same data set. Disregarding the slight systematic shifts of output radial distances, which can be easily accounted for by a global shift of the model predictions, it can be seen that the model performances are quite comparable. The respective standard deviations are about 0.69 $R_E$ and 0.65 $R_E$ for our NN-based model and for the *Shue et al.* [1998] model, respectively. We note, however, that despite the separation on the training and testing data subsets, the crossings obtained by the same spacecraft are used both for the training and testing of the model. This may possibly provide it some advantage over the *Shue et al.* [1998] model based on different spacecraft data in a different epoch.

Figure 4a shows the distance of the solar wind magnetopause as a function of dynamic pressure for IMF $B_z = 0$. The black curve corresponds to the NN model output, while the red curve is the dependence assumed by the empirical model by *Shue et al.* [1998]. It can be seen that while the NN correctly predicts the magnetopause radial distance to decrease with increasing solar wind dynamic pressure, the predicted dependence is not as steep as expected. We also note the lack of dependence for very high values of the solar wind dynamic pressure, which is due to these dynamic pressure values being critically under-sampled in the training data set. Figure 4b uses the same format as Figure 4a to investigate the dependence on IMF $B_z$ for a fixed value of $p_d = 1.63$ nPa (corresponding roughly to the median dynamic pressure value over the entire data set). No clear trend can be identified, with most of the observed variations taking place around IMF $B_z = 0$, in line with the low number of samples with very low/high values in the training data set.

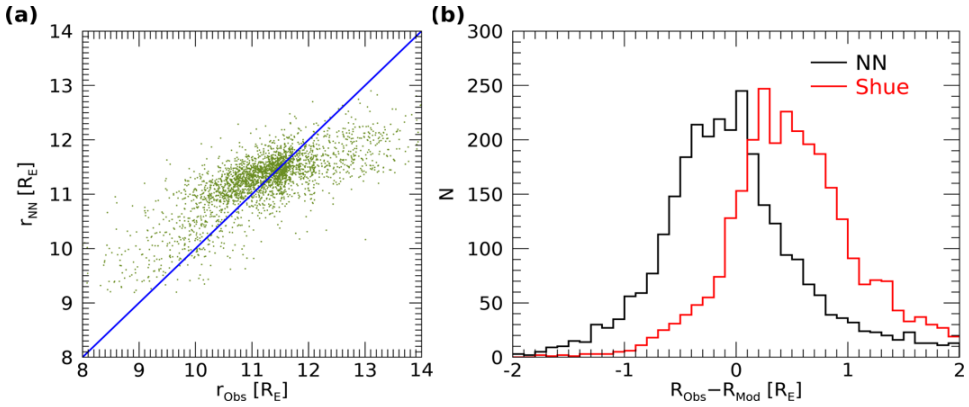


**Figure 3.** (a) Magnetopause distances predicted by neural network model as a function of the distances of the observed magnetopause crossings. The blue line shows a 1:1 dependence. (b) Histogram of the differences between the observed and model magnetopause distances obtained by the neural network model (black line) and the *Shue et al.* [1998] empirical model (red line).

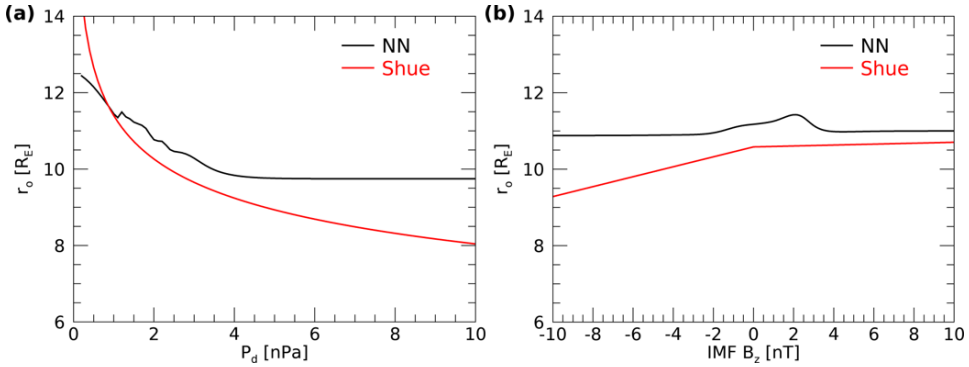


**Figure 4.** (a) Magnetopause distances in the subsolar point ($\theta = 0$) predicted by our NN-model (black curve) and by the *Shue et al.* [1998] empirical model (red curve). (a) As a function of the solar wind dynamic pressure for IMF $B_z = 0$. (b) As a function of IMF $B_z$ for $p_d = 1.63$ nPa.

## Discussion

The used data set of nearly 15,000 subsolar magnetopause crossings is quite unique and allows for extensive statistical studies. It is important to note that, due to the near-ecliptic latitudes of the crossings, they are essentially unaffected by the cusp indentations, and the assumption of the cylindrical symmetry of the situation is thus roughly valid. The main advantage of the used NN modeling approach is that it does not require any additional assumptions concerning the magnetopause shape. Moreover, it is very versatile and can be in the future easily extended to include other possible controlling parameters. For the moment, we considered only two solar wind parameters, i.e., the solar wind, dynamic pressure, and IMF $B_z$. Considering the assumed cylindrical symmetry, the location of the model magnetopause crossing is characterized exclusively by the angle $\theta$. This can be again easily extended in the future to study possible magnetopause asymmetries.

The NN utilized in the study consisted of two hidden layers, with each layer comprising 15 neurons. This was determined based on experiments with varying the number of neurons in each hidden layer (and also the number of the hidden layers) to optimize the prediction precision. We note, however, that the NN performance did not seem to crucially depend on these factors, as long as the number of neurons is not too low or too high. Another free parameters which may be possibly tuned in the future are the functions used for the normalization of the input parameters and/or neurons in the other layers. This seems to be a possible way how to avoid some of the issues regarding the steepness of the model prediction as a function of the solar wind dynamic pressure. The aforementioned insufficient steepness of the NN model as a function of the solar wind dynamic pressure is the reason for the observed overfitting

at low radial distances and underfitting at higher radial distances. Based on a simple evaluation of the pressure balance across the magnetopause, one might expect the subsolar magnetopause stand-off distance $r_0$ to vary with the dynamic pressure as $r_0 \propto p_d^{-1/6}$. Such an exponent was considered, e.g., by *Boardsen et al.* [2000], while *Shue et al.* [1998] analysis indicated a value of the exponent equal to $-1/6.6$. Although the proper exponent value is thus somewhat unclear, the steepness resulting from the NN approach is obviously lower than it should be (corresponding to a larger exponent value). This is likely due to two somehow related issues: i) there is a lack of magnetopause crossings obtained at high values of $p_d$, resulting in a rather flat dependence at high solar wind dynamic pressures and generally not so steep slope, and ii) the applied normalization of the input data causes problems when the distribution of a given input parameter has a significant long tail, as the tail is effectively suppressed by the normalization. Different normalization procedures of the dynamic pressure are to be used in the future to tackle this issue. The obtained dependence on the IMF $B_z$ is only rather weak and its general trend does not seem to much correspond to the *Shue et al.* [1998] model dependence. This may be possibly in line with recent studies suggesting that the IMF magnitude is actually more important [*Li et al.*, 2023]. This parameters is yet to be considered in the future version of the NN model.

## Conclusions

We used as many as about 15,000 magnetopause crossings within 30° from the subsolar point identified in the THEMIS A–E, Magion 4, Geotail, and Interball satellite data to investigate the possibility of modeling the magnetopause radial distance using a NN. We assumed a cylindrical symmetry around the axis of the incoming solar wind, expressing the magnetopause crossing location (on top of the predicted radial distance) exclusively by the angle $\theta$ between the positional vector of a given crossing and the direction toward the impinging solar wind. Two solar wind parameters believed to be the most important for controlling the magnetopause location were considered: i) solar wind dynamic pressure $p_d$, and ii) IMF $B_z$. The constructed NN thus had three inputs and a single output, corresponding to the predicted magnetopause radial distance. The resulting model shows a correlation of 0.74 with the testing magnetopause crossing distances. Although this is quite comparable to the correlation obtained for a widely used *Shue et al.* [1998] empirical model with the same parameterization (0.75), the applied method allows for significant further improvements. The model is overfitting at low radial distances and underfitting at higher radial distances. This can be possibly solved by a better normalization of the solar wind dynamic pressure before using it as a NN input. Moreover, the used approach can be easily extended to use more input parameters, gaining direct data-driven insight into the factors controlling the magnetopause distance.

## References

Aghabozorgi, M., Němec, F., Pi, G., Němeček, Z., Šafránková, J., Grygorov, K., and Šimůnek, J., Interplanetary Magnetic Field $B_y$ Controls the Magnetopause Location, *Journal of Geophysical Research*, *128*, 2023.

Boardsen, S. A., Eastman, T. E., Sotirelis, T., and Green, J. L., An empirical model of the high-latitude magnetopause, *Journal of Geophysical Research*, *105*, 23 193–23 219, 2000.

Cahill, L. J. and Amazeen, P. G., The boundary of the geomagnetic field, *Journal of Geophysical Research*, *68*, 1835–1843, 1963.

Case, N. A. and Wild, J. A., The location of the Earth's magnetopause: A comparison of modeled position and in situ Cluster data, *Journal of Geophysical Research: Space Physics*, *118*, 6127–6135, 2013.

Dušík, Š., Granko, G., Šafránková, J., Němeček, Z., and Jelínek, K., IMF cone angle control of the magnetopause location: Statistical study, *Geophysical Research Letters*, *37*, 2010.

Eastman, T., Boardsen, S. A., Chen, S. H., Fung, S. F., and Kessel, R. L., Configuration of high-latitude and high-altitude boundary layers, *Journal of Geophysical Research*, *105*, 23 221–23 238, 2000.

Fairfield, D. H., Average and unusual locations of the Earth's magnetopause and bow shock, *Journal of Geophysical Research*, *76*, 6700–6716, 1971.

Formisano, V., Domingo, V., and Wenzel, K.-P., The three-dimensional shape of the magnetopause, *Planetary and Space Science*, *27*, 1137–1149, 1979.

Kohonen, T., *Self-Organization and Associative Memory*, Springer-Verlag Berlin Germany, 1989.

Lavraud, B., Larroque, E., Budnik, E., Génot, V., B, J. E., Dunlop, M. W., Foullon, C., Hasegawa, H., Jacquey, C., Nykyri, K., et al., Asymmetry of magnetosheath flows and magnetopause shape during low Alfvén Mach number solar wind, *Journal of Geophysical Research*, *118*, 1089–1100, 2013.

Li, S., Sun, Y. Y., and Chen, C.-H., An interpretable machine learning procedure which unravels hidden interplanetary drivers of the low latitude dayside magnetopause, *Space Weather*, *21*, e2022SW003 391, 2023.

Lin, R. L., Zhang, X. X., Liu, S. Q., Wang, Y. L., and Gong, J. C., A three-dimensional asymmetric magnetopause model, *Journal of Geophysical Research*, *115*, A04 207, 2010.

Liu, Z. Q., Lu, J. Y., Wang, C., Kabin, K., Zhao, J. S., Wang, M., Han, J. P., Wang, J. Y., and Zhao, M. X., A three-dimensional high Mach number asymmetric magnetopause model from global MHD simulation, *Journal of Geophysical Research*, *120*, 5645–5666, 2015.

Lu, J., Liu, Z.-Q., Kabin, K., Jing, H., Zhao, M., and Wang, Y., The IMF dependence of the magnetopause from global MHD simulations, *Journal of Geophysical Research: Space Physics*, *118*, 3113–3125, 2013.

Lu, J. Y., Liu, Z. Q., Kabin, K., Zhao, M. X., Liu, D. D., Zhou, Q., and Xiao, Y., Three dimensional shape of the magnetopause: Global MHD results, *Journal of Geophysical Research*, *116*, 2011.

McCulloch, W. S. and Pitts, Walter, A., A logical calculus of the ideas immanent in nervous activity, *The bulletin of mathematical biophysics*, *5*, 115–133, 1943.

Nguyen, G., Aunai, N., Michotte de Welle, B., Jeandet, A., Lavraud, B., and Fontaine, D., Massive Multi-Mission Statistical Study and Analytical Modeling of the Earth's Magnetopause: 2. Shape and Location, *Journal of Geophysical Research*, *127*, e2021JA029 774, 2021a.

Nguyen, G., Aunai, N., Michotte de Welle, B., Jeandet, A., Lavraud, B., and Fontaine, D., Massive Multi-Mission Statistical Study and Analytical Modeling of the Earth's Magnetopause: 3. An Asymmetric Non Indented Magnetopause Analytical Model, *Journal of Geophysical Research*, *127*, e2021JA030 112, 2021b.

Němeček, Z., Šafránková, J., Lopez, R. E., Dušík, Š., Nouzák, L., Přech, L., Šimůnek, J., and Shue, J. H., Solar cycle variations of magnetopause locations, *Advances in Space Research*, *58*, 240–248, 2016.

Němeček, Z., Šafránková, J., and Šimůnek, J., An examination of the magnetopause position and shape based upon new observations, *Dayside magnetosphere interactions*, *248*, 135–151, 2020.

Petrinec, S. M. and Russell, C. T., Near-Earth magnetotail shape and size as determined from the magnetopause flaring angle, *Journal of Geophysical Research*, *101*, 137–152, 1996.

Šafránková, J., Němeček, Z., Dušík, Š., Přech, L., Sibeck, D. G., and Borodkova, N. N., The magnetopause shape and location: A comparison of the Interball and Geotail observations with models, *Annales Geophysicae*, *20*, 301–309, 2002.

Šafránková, J., Dušík, Š., and Němeček, Z., The shape and location of the high-latitude magnetopause, *Advances in Space Research*, *36*, 1934–1939, 2005.

Shue, J. H., Song, P., Russell, C. T., Steinberg, J. T., Chao, J. K., Zastenker, G., Vaisberg, O. L., Kokubun, S., Singer, H. J., Detman, T. R., et al., Magnetopause location under extreme solar wind conditions, *Journal of Geophysical Research*, *103*, 17 691–17 700, 1998.

Sibeck, D. G., Lopez, R. E., and Roelof, E. C., Solar wind control of the magnetopause shape, location, and motion, *Journal of Geophysical Research*, *96*, 5489–5495, 1991.

Spreiter, J. R., Summers, A. L., and Alksne, A. Y., Hydromagnetic flow around the magnetosphere, *Planetary and Space Science*, *14*, 223–253, 1966.

Svozil, D., Kvasnicka, V., and Pospichal, J., Introduction to multi-layer feed-forward neural networks, *Chemometrics and intelligent laboratory systems*, *39*, 43–62, 1997.

Tsyganenko, N., Modeling of twisted/warped magnetospheric configurations using the general deformation method, *Journal of Geophysical Research*, *103*, 23 551–23 563, 1998.

Verigin, M. I., Kotova, G. A., Bezrukikh, V., Zastenker, G., and Nikolaeva, N., Analytical model of the near-Earth magnetopause according to the data of the Prognoz and Interball satellite data, *Geomagnetism and Aeronomy*, *49*, 1176–1181, 2009.